Electronic Supplementary Material (ESI) for Nanoscale.

Supporting Information

Free charges versus excitons: photoluminescence investigation of InGaN/GaN multiple quantum well nanorods to their planar counterpart

Weijian Chen,[a] Xiaoming Wen,[b]* Jianfeng Yang,[a] Michael Latzel,[cd] Robert Patterson,[a] Shujuan Huang,[a] Santosh Shrestha,[a] Baohua Jia,[b] David Moss,[b] Silke Christiansen,[cef] and Gavin Conibeer[a]*

[a] *Australian Centre for Advanced Photovoltaics, School of Photovoltaic and Renewable Energy Engineering, UNSW Sydney, Sydney 2052, Australia.*
[b] *Centre for Micro-Photonics, Swinburne University of Technology, Melbourne 3122, Australia.*
[c] *Max Planck Institute for the Science of Light, Staudtstr. 2, 91058 Erlangen, Germany*
[d] *Institute of Optics, Information and Photonics, Friedrich-Alexander-Universität Erlangen-Nürnberg (FAU), Staudtstr. 7/B2, 91058 Erlangen, Germany*
[e] *Institute of Nanoarchitectures for Energy Conversion, Helmholtz-Zentrum Berlin für Materialien und Energie GmbH, Hahn-Meitner-Platz 1, 14109 Berlin, Germany*
[f] *Department of Physics, Freie Universität Berlin, Arnimallee 14, 14195 Berlin, Germany*

Section 1. Layer stack sample description

Figure S1. Layer description of the planar sample InGaN/GaN MQW (InGaN QWs with 18% In content).

Section 2. Experimental section and luminescence characterisation

Densely packed nanorods were fabricated by RIE using a silica nanosphere monolayer as an etching mask. Nanospheres with diameters of 700nm±4% and 500nm±4% were deposited on tops of the MQW layers by Langmuir-Blodgett (LB) deposition (Kibron Microtrough), which were subsequently shrunk into 500nm and 350nm in a $CF_4/SF_6/H_2$ plasma by inductively coupled plasma-reactive ion etching (ICP-RIE) (Oxford Instruments Plasmalab 100), respectively. A $CF_4/SF_6/H_2$ plasma was used for etching the MQW into nanorods array with the same diameter of the nanospheres and a height of 1.2µm. Dipped the samples in 5% HF solution for two minutes to remove the etching mask without damaging the nanorods.

For nanorod surface treatment, the as-etched nanorods were soaked in 8.5% aqueous KOH solution at room temperature for 75 minutes then rinsed with ultrapure water and dried by nitrogen gun. Al_2O_3 thin layers of 10 nm were coated by using atomic layer deposition (ALD) in a FlexAL (Oxford Instruments) ALD system at 200 °C using ultrapure water as a reactant and trimethyl aluminum (Al(CH3)3, purity > 98%, Strem Chemicals) as Al precursor.

The fluorescence lifetime imaging microscopy (FLIM) images, steady-state PL efficiency and TRPL decay traces were done by a Micro Time 200 (Picoquant) confocal microscopy using TCSPC technique with an excitation of the 405nm laser, using a bandpass filter at 442nm. The use of 405nm laser guarantees an excitation of the InGaN MQWs only. The laser light was focused through a water immersion objective (NA1.2), and the diameter of the excitation spot is estimated to be 215nm by $d = 2\omega_0 = \frac{2\lambda}{\pi NA}$ according to Gaussian profile. The number of pixels is 1024×1024 in all FLIM images. All PL measurements were undertaken at room temperature.

Figure S2 & Figure S3 presents the morphology and luminescence uniformity of the nanorods array.

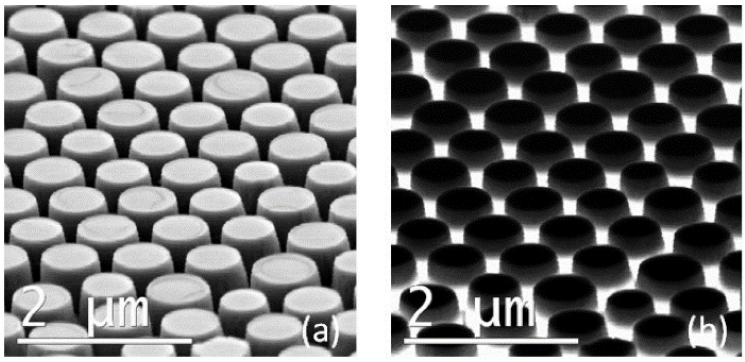

Figure S2. (a)SEM image of the large nanorods and (b) the corresponding monochromatic CL mapping of the nanorods at the InGaN/GaN MQW luminescence (442 nm)

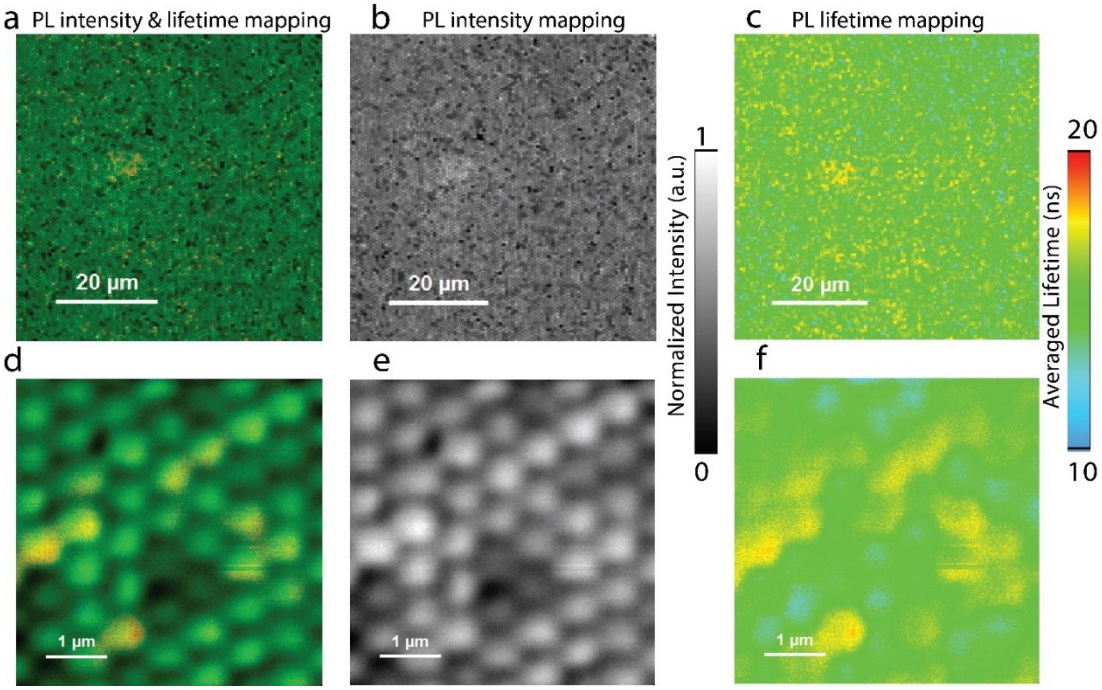

Figure S3. (a)&(d) FLIM images of the large nanorods; (b)&(e) PL intensity mapping and (c)&(f) PL lifetime mapping of the same area in (a)&(d).

Section 3. PL spectra of InGaN/GaN MQW planar and nanorod samples

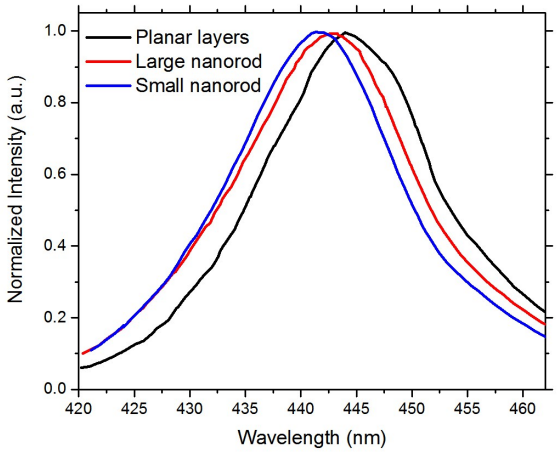

Figure S4. PL spectra of InGaN/GaN MQW planar and nanorod samples

Section 4. Mechanism analysis of PL enhancement in nanorods

This PL enhancement in the nanorods has been attributed to various reasons, including strain relaxation, higher light extraction efficiency, and lateral carrier confinement.

The strain relaxation in InGaN/GaN nanorods was commonly determined by the luminescence blue-shift. Compared to the planar MQWs, the luminescence peak was blue-shifted in the nanorods (Figure S2). Such strain relaxation is also confirmed by the authors' previous publications[1,2] using micro-Raman measurement. The relaxation of strain in turn

reduces the band bending and delocalization of carriers. Hence the carriers are both more localized and more likely to recombine radiatively.

There is a light in-coupling enhancement (often referred as an optical absorption enhancement), resulted from the effective refractive index of the nanoarrays as an assemble.[3,4] Light extraction efficiency is also enhanced in nanorods due to the reduced light reflection and enhanced waveguide effect to extract photons in the longitudinal direction. To verify this argument, light extraction efficiency is simulated using Finite-difference time-domain (FDTD) method by measuring the upward radiation power from a single dipole source in a nanorod. Figure S3 (a) illustrates the model structure for the FDTD simulation, where perfect conducting layers (PCL) are added in the x-y directions as total reflection layers and perfectly matched layers (PMC) are added above and below the nanorods as total absorption layer. Two transmission monitors detect the upward and downward radiation power, respectively. In this work, we are only interested in the upward radiation power as it is detectable by the PL measurement. As shown in Figure S3 (b), a spatial averaged light outcoupling efficiency is about 20%, which is more than 5 times higher compared to that of the planar MQWs (3%). Although this simulation is quite coarse as the refractive index of the InGaN/GaN MQW and GaN are based on literature estimation, it is safe to conclude that the enhanced light out-coupling efficiency plays an important role in the PL enhancement.

While much larger than the Bohr radius, the size of the nanorods are comparable to the diffusion length in InGaN quantum well. Such that the photogenerated carriers in nanorods are laterally confined within the rod area compared to planar layers, which significantly enhances the electron-hole oscillator strength. The radiative recombination rate is therefore much higher in the nanorods than the planar layers, which results in the superior competition with non-radiative recombination, even though defect densities are higher than the planar layers.

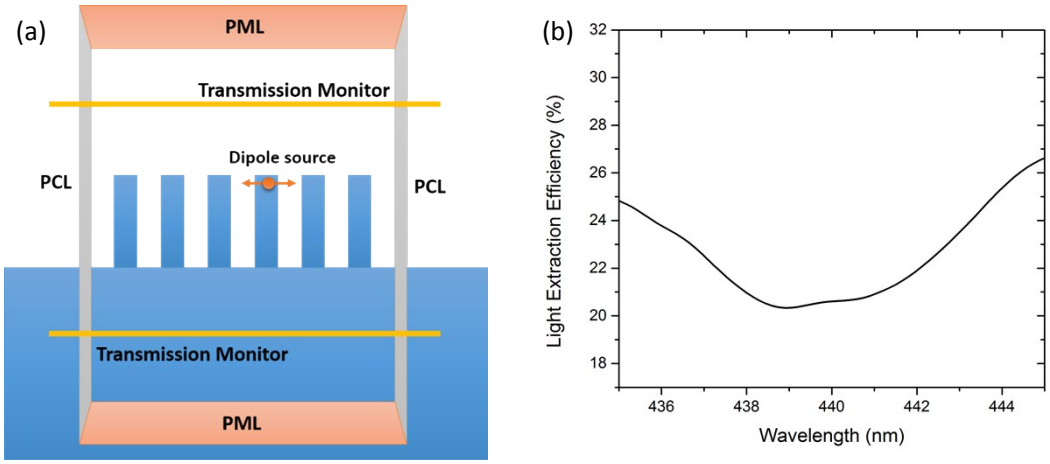

Figure S5 (a) Model structure for simulating light extraction efficiency and (b) the calculated light extraction efficiency at different wavelength.

Section 5. Injected carrier density calculation

The methodology of calculating the injected carrier density is referred to Liu et al:[5]

$$n_{injected} = \frac{PD}{(h\upsilon)\cdot d_{InGaN}\cdot f}\cdot\left[1-\exp\left(-\alpha_{InGaN}d_{InGaN}\right)\right]\cdot(1-R) \quad (1)$$

Here PD is the power density of the excitation laser, incident photon energy ($h\upsilon$)=3.06eV, InGaN/active layer total thickness: d_{InGaN}=25nm (shown Figure S1), laser repetition rate=10Mhz. Absorption coefficient $\alpha_{InGaN} = 10^4\ cm^{-1}$ is referred in Ambacher et al.[6] Reflectance is determined by reflection measurement as shown in Figure S4: R_{planar}=27%, $R_{nanorod}$=16%.

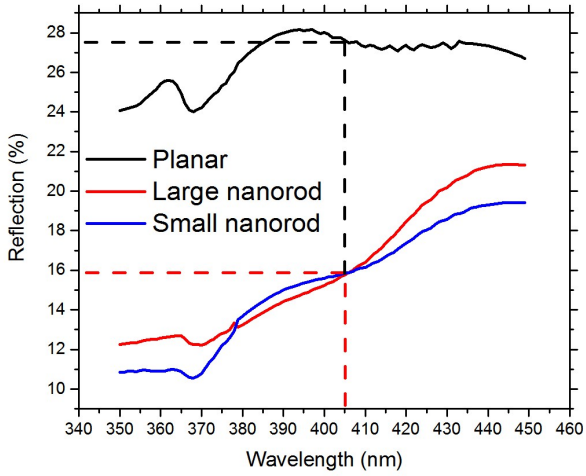

Figure S6. Reflection of planar and nanorod samples

Quasi-planar absorption behaviour in nanorods applied in this carrier density calculation:

In the nanoscale resolved PL measurement, a single nanorod with a diameter of 350nm /500nm should be considered rather than a nanorod array. All steady-state and time-resolved PL experiments in this paper were undertaken using a confocal microscopy, where excitation light was focused into an area with a diameter less than 300 nm. The excitation spot size is smaller than the single nanorod area, and all PL excitations were carefully focused at the center of each nanorod. Besides, there is no resonance induced absorption enhancement in this structure at the wavelength of excitation laser (405nm). One single nanorod can be approximated to have a quasi-planar absorption behaviour when calculating the photo-excited carrier density. Considering that the diameter of the nanorods is of the same order of magnitude as the excitation wavelength, the effective refractive index of the nanorod should be used, which is accounted for by using the effective reflectance.

Section 6. The modified rate equation model derivation

The photogenerated carriers in the InGaN MQW are assumed to comprise of excitons and free carriers. The equilibrium of the carrier population is established right after the excitation pulse by interparticle collisions, which is on a timescale of femtoseconds and much faster than the carrier recombination.[7] The total density of photogenerated carriers is described as:

$$n = n_x + n_{eh} = a_x n + a_{eh} n, \qquad (2)$$

where a_x and a_{eh} represent the portion of excitons density (n_x=$a_x n$) and free carrier density (n_{eh}= $a_{eh} n$), respectively. The portions of exciton/free carrier population, a_x and a_{eh}, are independent of the injected density at room temperature below the Mott density.[7]

The rate equation used to describe the dynamics of free electron-hole dynamics alone in InGaN/GaN MQWs is given as:[7]

$$-\frac{dn_{eh}}{dt} = A_{eh} n_{eh} + B_{eh} n_{eh}^2, \quad (3)$$

where A_{eh} and B_{eh} are the Shockley-Read-Hall and radiative recombination coefficient of electron-hole, respectively.

The exciton recombination, as described by Chichibu, S. F. et al.,[8] should follow the rate equation,

$$-\frac{dn_x}{dt} = A_x n_x + B_x n_x, \quad (4)$$

where A_x and B_x are the corresponding non-radiative and radiative recombination coefficients of excitons, respectively.

Generalizing equation (2)(3)(4), we have the following equation to examine the total carrier dynamics in the InGaN MQW:

$$-\frac{dn}{dt} = (A_{eh} a_{eh} + A_x a_x) n + B_x a_x n + B_{eh} a_{eh}^2 n^2, \quad (5)$$

To simplify equation (5), we define the generalized coefficients of nonradiative recombination as $A' = A_{eh} a_{eh} + A_x a_x$, radiative recombination of free electron-hole as, $B'_{eh} = B_{eh} a_{eh}^2$, and radiative recombination of exciton as: $B'_x = B_x a_x$.

The final dynamics equation with generalized recombination coefficients applies to the in the InGaN MQW is:

$$\frac{dN}{dt} = \frac{\alpha I_{ex}}{h\nu_{ex}} - A'N - \eta B'_x N - \eta B'_{eh} N^2 \quad (6)$$

Two additional terms are included in Equation (6) to fit our experimental setup: η is an output coupling coefficient considering a finite luminescence detection; $\frac{\alpha I_{ex}}{h\nu_{ex}}$ is the excitation rate while α is the light absorption, $h\nu_{ex}$ is the single photon energy of the incident light, and I_{ex} is the excitation power; N is the total carrier density.

Under steady state, we have $\frac{dN}{dt} = 0$, thus equation (6) can be rearranged into:

$$I_{ex} = \frac{h\nu_{ex}}{\alpha}(A'N + \eta B'_x N + \eta B'_{eh} N^2) \quad (7)$$

The emitted PL power density can then be described as

$$I_{em} = \eta h\nu_{em}(B'_x N + B'_{eh} N^2) \quad (8)$$

Based on equation (7) & (8), the PL efficiency can be expressed as:

$$PL_{eff}(N) = \beta \frac{B'_x N + B'_{eh} N^2}{A'N/\eta + B'_x N + B'_{eh} N^2} \quad (9)$$

where β is a constant to absorb all the other coefficients.

A discussion of the limitations in this model:

The parameters $\alpha, \beta \,\&\, \eta$ are inherent properties of each sample, and it is difficult to accurately determine their absolute values in order to make comparisons meaningful. However, this is NOT the intention of our work or our model. Since the radiative recombination rates of free charges and excitons are equally impacted by these parameters (equation 9), the ratio between the free charges and exciton recombination rates $B_{eh}^{'}N^2/(B_x^{'}N)$ is not affected by the absolute values of $\alpha, \beta \,\&\, \eta$. Therefore, any comparison between different samples using such a ratio is valid. This leads to our experimental observation that excitons dominate in the planar layers while free carrier recombination displays an important role in the nanorods. Please note that the comparison between each sample does not need to rely on any direct comparison of the absolute value of PL efficiency between the samples. Our conclusions are based on our observation of the different carrier density dependence between the planar layers and nanorods.

Section 7. FLIM image of the sparse nanorods samples

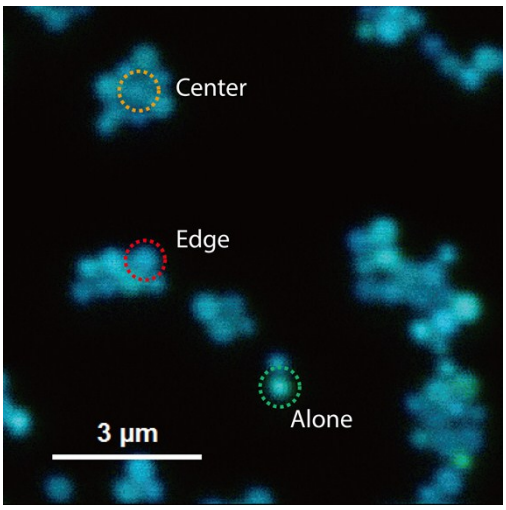

Figure S7. FLIM image of the sparse nanorods samples

Section 8. Trap state density determination

Under low excitation ranges where the Auger recombination is negligible, the photoexcited carrier dynamics can be described by:[9]

$$\frac{dn(t)}{dt} = -\sum_i a_i n(t) n_{tp}^{i}(t) - \frac{n(t)}{\tau_0} \qquad (10)$$

where $n_{tp}^{i}(t)$ is the trap states density, a_i is the product of the trapping cross section and the carrier velocity and τ_0 is the averaged radiative lifetime. The first term in (10) denotes various trap non-radiative recombination channels while the section term represents the radiative recombination.

The steady-state PL intensity can be derived from the second term of (10):

$$I_{PL} = k \int_0^{\infty} \frac{n(t)}{\tau_0} dt \quad (11)$$

where *k* is an amplitude coefficient.

From equation (10) (11), the injected carrier density $n(0)$ can be calculated as:

$$n(0) = \sum_i n_{tp}^{i}(0)\left(1 - exp(-a_i \tau_0 \frac{I_{pl}}{k})\right) + \frac{I_{pl}}{k} \quad (12)$$

When the PL from the quantum well is strong enough, equation (12) could be simplified to:

$$n(0) = \sum_i n_{tp}^{i}(0) + \frac{I_{pl}}{k} \quad (13)$$

By fitting the injected carrier density dependent steady-state PL, the overall defects density can be estimated. In the case of InGaN/GaN MQW nanorod, the total defect density includes the in-plane defects in the quantum well and the surface defects at the nanorod sidewall. The trap state density within the MQW can be accurately estimated from the steady-state PL of the InGaN\GaN MQW layer stacks where there are no rod-edge surface defects. Then the surface trap state densities can be calculated accordingly.

REFERENCES

1 G. Sarau, M. Heilmann, M. Latzel and S. Christiansen, *Nanoscale*, 2014, **6**, 11953–62.

2 M. Latzel, P. Büttner, G. Sarau, K. Höflich, M. Heilmann, W. Chen, X. Wen, G. Conibeer and S. H. Christiansen, *Nanotechnology*, 2017, **28**, 55201.

3 J. Zhu, Z. Yu, G. F. Burkhard, C.-M. Hsu, S. T. Connor, Y. Xu, Q. Wang, M. McGehee, S. Fan and Y. Cui, *Nano Lett.*, 2009, **9**, 279–282.

4 R. Jayaprakash, D. Ajagunna, S. Germanis, M. Androulidaki, K. Tsagaraki, a Georgakilas and N. T. Pelekanos, *Opt. Express*, 2014, **22**, 19555.

5 B. Liu, R. Smith, M. Athanasiou, X. Yu, J. Bai and T. Wang, *Appl. Phys. Lett.*, 2014, **105**.

6 O. Ambacher, D. Brunner, R. Dimitrov, M. Stutzmann, A. Sohmer and F. Scholz, *Japanese J. Appl. Physics, Part 1 Regul. Pap. Short Notes Rev. Pap.*, 1998, **37**, 745–752.

7 W. Liu, R. Butté, A. Dussaigne, N. Grandjean, B. Deveaud and G. Jacopin, *Phys. Rev. B*, 2016, **94**, 195411.

8 S. Nakamura and S. F. Chichibu, *Introduction to nitride semiconductor blue lasers and light emitting diodes*, CRC Press, 2000.

9 G. Xing, N. Mathews, S. S. Lim, N. Yantara, X. Liu, D. Sabba, M. Grätzel, S. Mhaisalkar and T. C. Sum, *Nat. Mater.*, 2014, **13**, 476–480.